Meteorologische Zeitschrift, PrePub DOI 10.1127/metz/2015/0653

Impact of topography on the diurnal cycle of summertime moist convection in idealized simulations

Hanieh Hassanzadeh[1], Jürg Schmidli[1], Wolfgang Langhans[2], Linda Schlemmer[1*] and Christoph Schär[1]

[1]Institute for Atmospheric and Climate Science, ETH Zurich, Switzerland
[2]Earth Sciences Division, Lawrence Berkeley National Laboratory, USA

(Manuscript received October 14, 2014; in revised form May 13, 2015; accepted May 20, 2015)

Abstract

The impact of an isolated mesoscale mountain on the diurnal cycle of moist convection and its spatial variation is investigated. Convection-resolving simulations of flow over 3D Gaussian-shaped mountains are performed for a conditionally unstable atmosphere under diurnal radiative forcing. The results show considerable spatial variability in terms of timing and amount of convective precipitation. This variability relates to different physical mechanisms responsible for convection initiation in different parts of the domain. During the late morning, the mass convergence from the radiatively driven diurnal upslope flow confronting the large-scale incident background flow triggers strong convective precipitation over the mountain lee slope. As a consequence, instabilities in the boundary layer are swept out by the emerging cold pool in the vicinity of the mountain, and some parts over the mountain near-field receive less rainfall than the far-field. Over the latter, an unperturbed boundary-layer growth allows for sporadic convective initiation. Still, secondary convection triggered over the leading edge of the cold pool spreads some precipitation over the downstream near-field. Detailed analysis of our control simulation provides further explanation of this frequently observed precipitation pattern over mountains and adjacent plains. Sensitivity experiments indicate a significant influence of the mountain height on the precipitation pattern over the domain.

Keywords: Moist convection, Precipitation, Diurnal cycle, Topography, Idealized studies, Summertime

1 Introduction

Mountain ranges strongly influence the distribution of precipitation, both in space and time (Banta, 1990; Roe, 2005; Houze, 2012). This affects the distribution of water resources and may cause droughts or floods in the surrounding regions. Mountain-induced vertical lifting may lead to precipitation, either by adiabatic cooling and condensation, or by triggering moist convection. Hence, numerous studies have been done to understand the role of mountains in modifying the overlaying flow pattern (e.g. Queney, 1948; Smith, 1979; Durran, 1990).

Whether the flow goes over or around the mountain dramatically changes the atmospheric processes over the mountain's near field (Smith and Gronas, 1993; Schär, 2001). For dry flow past intermediate-scale elliptical mountains, the atmospheric flow regime depends mostly on two non-dimensional parameters: the non-dimensional mountain height ($\hat{h} = HN/U$; in which H is the mountain height, U is the background wind speed and N is the Brunt-Väisälä frequency) and a shape parameter $\beta = A_x/A_y$, the ratio of along-flow to perpendicular-to-flow characteristic width of the mountain. Thus, dry flows pose less complexity and have been investigated comprehensively from many points of view (e.g. Bauer et al., 2000; Crook and Tucker, 2005; Schär and Durran, 1997). However, for moist flows, the flow regime may change non-linearly from stable to conditionally unstable by reshaping the temperature profile through dynamical effects, thereby leading to condensational heating in clouds. The effect of conditional instability is represented by N_m, the moist Brunt-Väisälä frequency, and brings some complexity to the modeling of the moist flows (Miglietta and Buzzi, 2001; Kirshbaum and Smith, 2008). Due to this complexity the influence of humidity on the impinging flow over topography has yet to be investigated in full detail.

Some basic precipitation-formation processes over mountains have been studied using highly simplified and idealized 2D/3D frameworks (Schneidereit and Schär, 2000; Kirshbaum and Durran, 2004; Miglietta and Buzzi, 2004; Smith and Barstad, 2004; Fuhrer and Schär, 2005; Miglietta and Rotunno, 2009). These simplified frameworks reduce the degrees of freedom and allow a comparison to analytical models. Despite the relevance of such studies, some of the factors neglected in the simplifications are of importance, particularly at longer time-scales. For instance, some of the previous studies neglected surface and boundary layer processes as well as radiative forcing.

However, radiative forcing is the strongest driver of the diurnal cycle (DC). It regulates the amount of avail-

*Corresponding author: Linda Schlemmer, Institute for Atmospheric and Climate Science, Universitätsstrasse 16, ETH Zurich, CH-8092 Zurich, Switzerland, e-mail: linda.schlemmer@env.ethz.ch

able energy within the planetary boundary layer (PBL) and affects the flow regime by redefining the vertical stratification. Considering radiative forcing, Mayr and Armi (2010) showed the significant influence of the diurnal heating on the Sierra Nevada downstream flow. Demko and Geerts (2010a); Demko and Geerts (2010b) aimed at an improved understanding of the mountain circulation and its effect on orographic convective rainfall in the DC framework. While their simulations were designed to capture most of the involved physics for a specific event, their setup was used to study only a short (3 individual days) period in time.

It has also been shown that capturing convection initiation (CI) precisely is a key factor in forecasting the timing and amount of precipitation (Kottmeier et al., 2008). Thus, a series of studies was initiated within the Convective and Orographically-induced Precipitation Study (COPS) over southern Germany and eastern France (Wulfmeyer et al., 2011) to investigate the effect of the surface fluxes, soil moisture, wind profile, water vapor, and stratification on the timing, location, and amount of convection and precipitation over complex terrain (Barthlott and Kalthoff, 2011; Barthlott et al., 2011; Bennett et al., 2011; Eigenmann et al., 2011; Hagen et al., 2011; Hauck et al., 2011; Van Baelen et al., 2011).

In a recent study of the DC of warm-season precipitation, Bao and Zhang (2013) studied the initiation and development of convection over northern China. They found that in addition to the impact of the mountain-plain circulation, cold-pool dynamics play an important role in defining the precipitation pattern over the plain adjacent to the Yanshan-Taihangshan mountain ranges. The development of cold pools over a sea surface in the tropics has e.g. been studied by Addis et al. (1984), Young et al. (1995), and Tompkins (2001) and in the midlatitudes over continental areas by Weaver and Nelson (1982) and Schlemmer and Hohenegger (2014). Moreover, cold pools play an imporant role in the organization of multicell storms or squall-lines through the dynamical impact at their leading edge (Parker, 1996; Rotunno et al., 1988).

Most of the previous studies on CI over mountainous terrain have focused on single days, where the development of convection is to a large degree determined by the ambient conditions. In order to capture the feedbacks of convection onto the environment, Schlemmer et al. (2011) (hereafter S2011) established an idealized framework to examine the DC of midlatitude summertime moist convection over flat terrain and its evolution into an equilibrium state. They termed the emergent state "diurnal equilibrium". With diurnal equilibrium an equilibrated DC of the land-atmosphere system is addressed, which is reflected in little day-to-day variability of the DC of surface precipitation (Betts, 2000), rather than in the equilibrium between the large-scale forcing and the small-scale convective response as in Arakawa and Schubert (1974). This diurnal equilibrium is not considered in short-term event-based case studies. Schlemmer et al. (2012) explored this equilibrium state and studied its sensitivity to soil moisture and atmospheric stability.

The current paper investigates the DC of summertime precipitation and moist convection over 3D topography extending the framework of S2011. The simulations use a convection-resolving model with a grid spacing of 2 km. Previous studies have shown that this resolution appropriately resolves the vertical fluxes of moisture, heat, and momentum associated with organized deep convection (Hohenegger et al., 2008; Schlemmer et al., 2011).

The main goal of the current study is to understand the spatial variability of the diurnal-equilibrium state of a conditionally unstable flow over an isolated mesoscale mountain in a setting resembling midlatitude summertime conditions. In order to understand the processes which govern the development and spatial diversity of convection, the evolution of the PBL and the processes in the free atmosphere are investigated in specific parts of the domain. An analysis of the mechanisms involved in the convection initiation and development in different regions of the mountainous domain is presented. In addition, the influence of the mountain height on the convection initiation and development over the near field is investigated from a temporal and spatial perspective.

The paper is organized as follows: Section 2 describes the experimental setup and the model used. Section 3 discusses the results. The conclusions are summarized in Section 4.

2 Experimental setup

2.1 Model description

The simulations are carried out using version 4.28 of the Consortium for Small-scale Modeling (COSMO) model (Baldauf et al., 2011) which is the pre-release version of the unified model version COSMO-CLM (CCLM) version 5.0. The CCLM is a nonhydrostatic limited-area model that solves the fully compressible Navier-Stokes equations using the split-explicit approach (Wicker and Skamarock, 2002). The time integration is done using a third-order Runge-Kutta scheme (see Förstner and Doms, 2004) with a fifth-order advection scheme for horizontal and vertical velocities, temperature, and pressure and a second-order Bott scheme (Bott, 1989) for the advection of moist quantities. CCLM (Steppeler et al., 2003; Doms and Förstner, 2004) includes a full parametrization package consisting of a prognostic turbulent energy-based scheme of order 1.5 (Raschendorfer, 2001), a radiation scheme (Ritter and Geleyn, 1992), a one-moment microphysics bulk scheme considering prognostic cloud water, cloud ice, precipitation, graupel and snow (Reinhardt and Seifert, 2006), and a surface-layer scheme based on turbulent kinetic energy (Mironov and Raschendorfer, 2001). The 10-layer

soil model TERRA_ML (Heise et al., 2003) is used to simulate the interactions between the land and the atmosphere. In contrast to S2011, soil moisture is prescribed throughout the simulation (Section 2.3).

2.2 Domain and topography

The model domain covers $400 \times 200 \times 50$ atmospheric grid points with a horizontal grid-spacing of 2 km. The atmospheric vertical grid-spacing ranges between 20 m near the ground and about 1 km at the model top (at 22 km). The time step is set to 20 s. Doubly-periodic lateral boundary conditions are used and the Coriolis force is neglected. The surface elevation is set to 500 m above mean sea level (representative of the Alpine foreland) and an isolated mountain is placed 250 km from the upstream boundary. The topography of the mountain is given by a circular Gaussian function:

$$h(x, y) = He^{-\frac{x^2+y^2}{A^2}} \qquad (2.1)$$

where H is the mountain height and A is the mountain half-width. For the control simulation (referred to as H1000), we use $A = 20\,\text{km}$ and $H = 1000\,\text{m}$. A simulation over flat terrain (FLAT) is run in addition with a setup identical to H1000, except for the absence of the topography.

2.3 Atmospheric and soil profiles and relaxation method

As in S2011, we use idealized profiles to drive our simulations. A single vertical sounding representative for summertime European climatological conditions taken from 48.25 ° N is applied to initialize temperature, relative humidity, and the horizontal wind components (Figure 1). The zonal wind is set to $2\,\text{m s}^{-1}$ at the surface, increases to $10\,\text{m s}^{-1}$ at the tropopause and decreases again to $-5\,\text{m s}^{-1}$ in the stratosphere, while the meridional wind speed is set to zero. To obtain a conditionally unstable stratification, a lapse rate of $-7\,\text{K km}^{-1}$ is considered for tropospheric temperature with a surface temperature of 291 K. The relative humidity profile is based on the climatology of Peixoto and Oort (1996) and similar to S2011, with values of 70 % close to the surface decreasing to 40 % in the upper troposphere. In the stratosphere values are set to 10 %. Incoming solar radiation is set to the conditions at 48.25 ° N (latitude of Munich) on 12th July throughout the whole simulation.

In contrast to S2011 the saturation of the soil layers is prescribed to a fixed value of 60 % for the uppermost layer, increasing to 100 % at a depth of 2.5 m. A fully interactive soil moisture was found to result in unrealistically high values of soil moisture over the mountain due to the high precipitation amounts and the neglect of lateral runoff in the land-surface model. The soil temperature fully interacts with the atmosphere.

White noise with an amplitude of ±1.0 K is added to the initial temperature of the first atmospheric layer

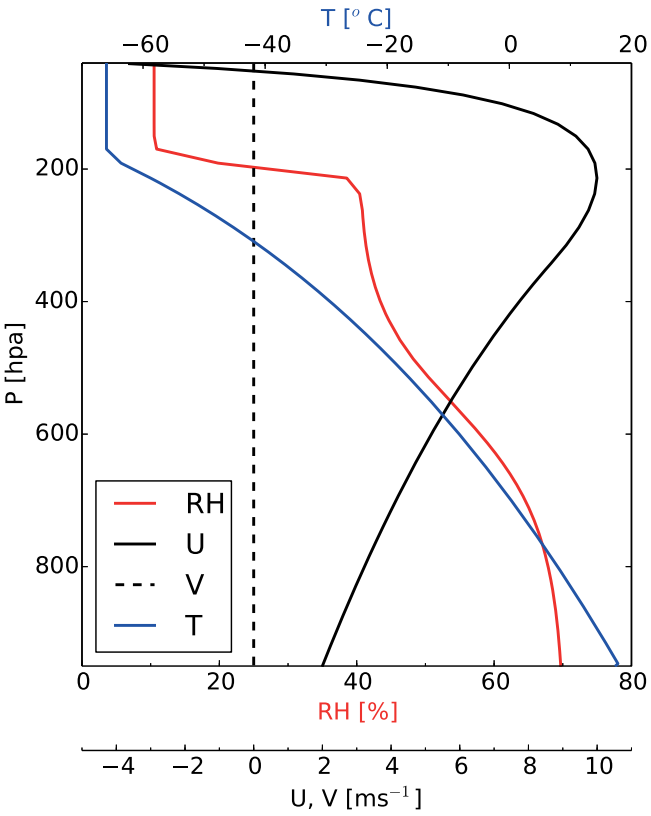

Figure 1: Initial profiles of the atmospheric temperature (blue), relative humidity (red) and horizontal wind components (black).

to break the symmetry of the horizontally homogeneous conditions. A Rayleigh damping sponge layer is implemented above 12 km to prevent gravity wave reflection.

Large-scale forcing is prescribed as in S2011. Domain mean values of temperature, specific humidity and horizontal wind are relaxed toward the reference profiles throughout the simulation. The relaxation factor is height-dependent in a way that the upper atmospheric state is relaxed with a time scale of $\tau = 1$ day while the lower layers run without relaxation. This setup allows for an unconstrained interaction between surface buoyancy fluxes, the boundary layer, and convection with the advective and radiative forcing. The relaxation is not applied to the soil temperature profiles since the deep soil temperature remains approximately constant throughout the simulation.

2.4 Equilibrium state

The simulations are run for 35 days. A quasi-steady state is reached after about 15 days. This is illustrated in Figure 2 for our control simulation, where the time series of the domain mean atmospheric temperature averaged over the 10 lowest layers (up to 750 m above the ground level (AGL)) as well as surface precipitation are shown. Hence, days 16–35 of the simulation are used to evaluate the diurnal equilibrium. The 20 days can be thought of an ensemble where each day is a realization of the same experiment with slightly different initial conditions.

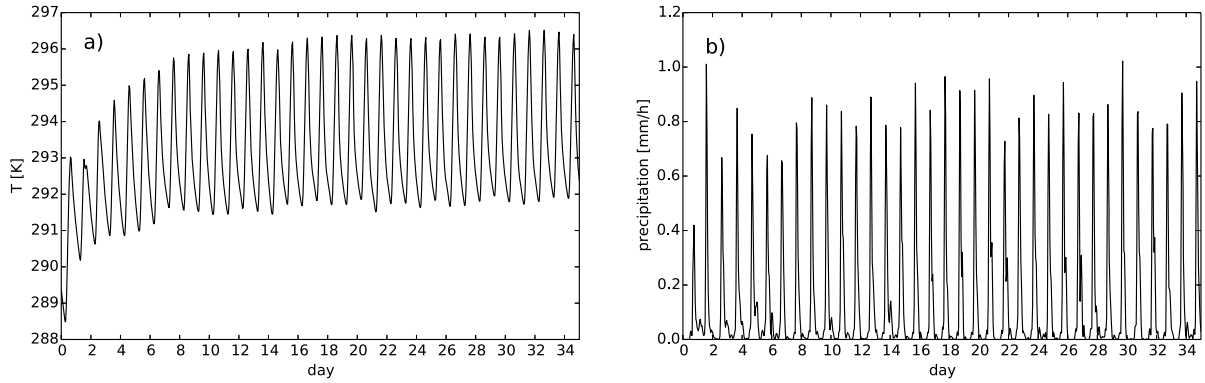

Figure 2: Time series of domain-mean (a) temperature for the 10 lowest atmospheric layers (up to 750 m) and (b) surface precipitation rate over 35 days of the control simulation.

In summary, our setup is similar to the CTL simulation in S2011, except for prescribed soil moisture, weaker background winds, a larger domain, and (of course) the mountain topography.

3 Results

3.1 Spatial diversity of precipitation and mean diurnal cycle

As shown in Figure 3, the presence of an isolated mountain leads to large spatial differences in the mean daily precipitation, ranging from 22.3 mm d^{-1} in the region of the lee-side maximum, to only 0.8 mm d^{-1} in the dry regions flanking the lee-side maximum. Mean precipitation in the mountain far field amounts to 3.1 mm d^{-1}. To have an estimate of the precipitation variation in different parts of the domain, Figure 4 presents along-flow variations of precipitation averaged in bands that represent the CENTER, FLANKS and DISTANT regions (see caption and Figure 3 for details). This illustrates heavy precipitation over the lee for CENTER, low precipitation near the obstacle for FLANKS, and almost uniform precipitation away from the obstacle for DISTANT.

For further analysis, we define three additional regions (see the red circles and box in Figure 3). The first region, WET, is centered around the precipitation maxima, the second region, DRY, is centered around the two precipitation minima, and the third region, FAR, is located several hundred kilometers downstream of the mountain.

In FLAT the evolution and spatial distribution of surface precipitation is more uniform. It resembles the convection evolution and precipitation pattern over FAR in H1000, where the effect of the topography is minimal (not shown). Further details on the DC of summertime moist convection over flat terrain are given in S2011 and Schlemmer et al. (2012) where also some sensitivity studies on the soil moisture, humidity, and atmospheric stratification over the flat terrain are presented.

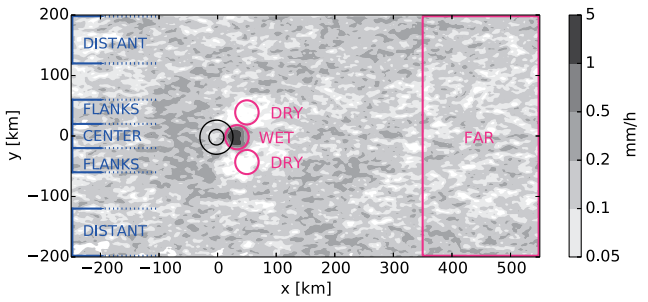

Figure 3: Mean surface precipitation rate (shading, 20-day mean) and mountain topography (black contours, at 250 and 750 m AGL). The blue brackets show the borders of the areas used for Figure 4. The red box and circles denote the three regions used for further analysis; the three circles have the radius of the mountain half-width, A, and are centered on the precipitation maxima for WET and on the two precipitation minima for DRY. The area of the regions are 1260, 2520, and 80000 km^2 for WET, DRY, and FAR, respectively.

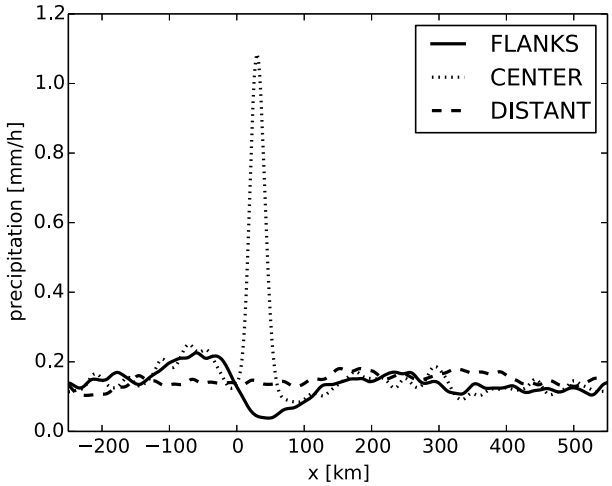

Figure 4: 20-day mean surface precipitation rate over the along-flow direction averaged in the y-direction for the areas shown in Figure 3 with blue colors.

The mean DC of clouds and precipitation for the three regions in H1000 and for the whole domain in

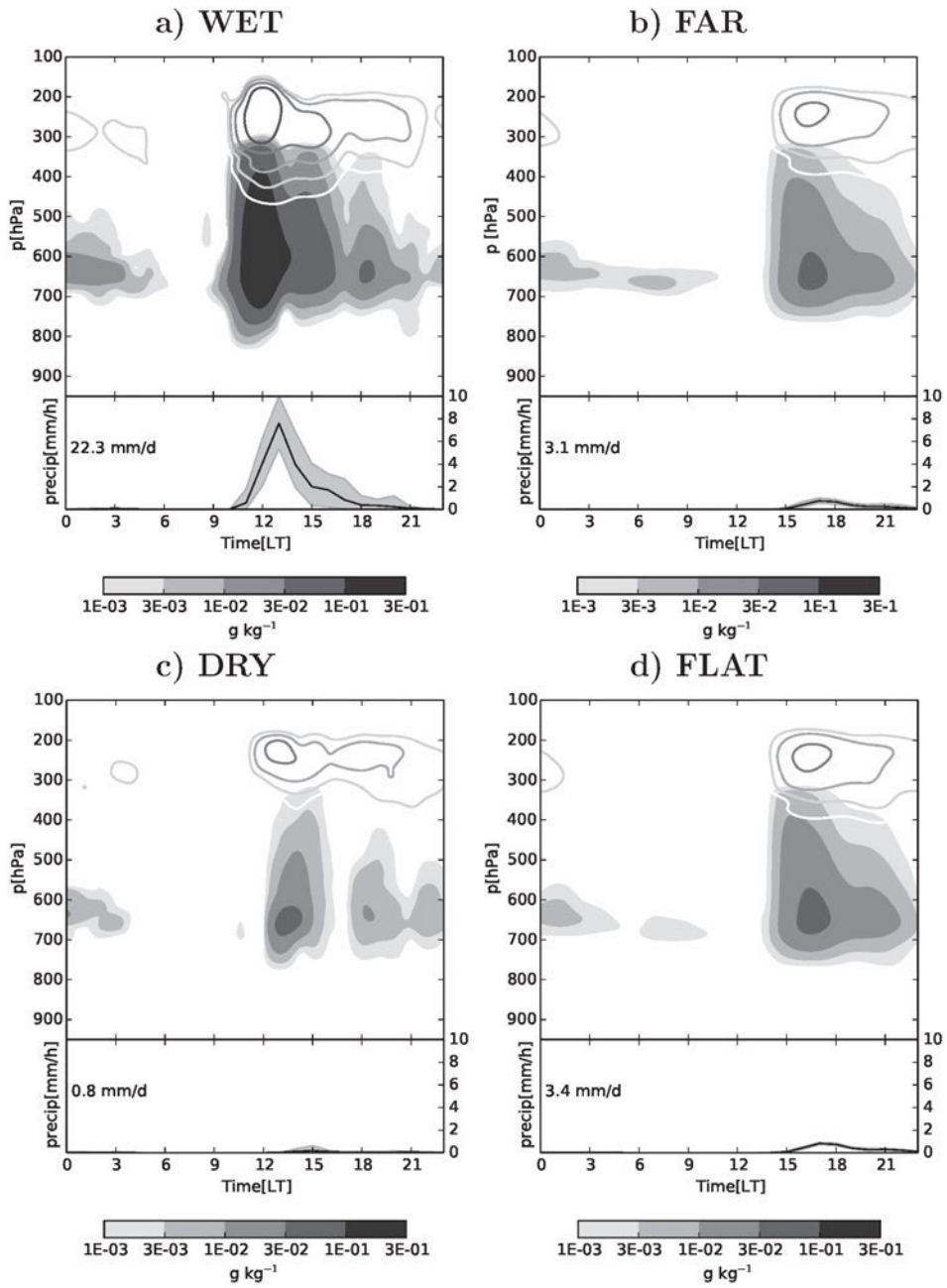

Figure 5: Mean diurnal cycle of clouds and precipitation over the three regions in H1000 (a–c) and the experiment without mountain (d). The upper part of the panels shows specific cloud liquid water content (g kg^{-1}, shading) and specific ice content (g kg^{-1}, contours, same intervals as shading). The lower part of the panels shows the mean diurnal cycle of the surface precipitation rate (solid line); the gray shading is the precipitation variability between the 10th and 90th percentile over the last 20 days of the simulation and the number in the lower panel is the daily mean precipitation amount.

FLAT is shown in Figure 5. The timing of cloud formation and precipitation generation differs remarkably for the three regions. While precipitation forms around 10:00 local time (1000 LT) over WET (Figure 5a), it triggers around 1500 LT over FAR (Figure 5b). The cloud-free period is several hours longer over DRY than over WET or FAR. The region-mean liquid water and ice content are much higher for WET, in particular around noon (Figure 5a). Furthermore, the mean daily precipitation amount is seven times higher over WET than over FAR. In contrast, DRY gets almost no precipitation (to be explained later). The highest liquid water and ice contents for the three regions are observed at 1200 LT over WET, at 1600 LT over FAR, and at 1300–1400 LT over DRY. In all regions, the precipitation peaks one hour after the clouds. The DC of clouds and precipitation over FLAT resembles the one over FAR (Figure 5b,d) which both are very similar to the DC obtained by S2011. In the morning boundary layer growth in response to surface heating triggers first convective cells. Throughout the afternoon, the collision of cold pools emerging from precipitating cells over the whole domain results in deep convection and precipitation (cf. Schlemmer et al., 2012; Schlemmer and Hohenegger, 2014).

3.2 Mean diurnal flow evolution and day-to-day variability

Figure 6 shows horizontal and vertical (at $y = 0$ km) distribution sof thermodynamic and dynamic quantities at certain local times (between 0800 to 1800 LT) and averaged over the 20 days to get a sense of the mean diurnal cycle.

At 0800 LT, upstream blocking and flow-around-the-mountain is observed (Figure 6a). This flow pattern as well as the vertically-propagating mountain-waves seen from the wind field in the upper panel result from the stable stratification. By 1000 LT (Figure 6b), a low-level moist convergence line emerges over the lee from the combination of the thermal (upslope) circulation and orographically-forced (background) flow (see, e.g. Banta, 1990). Thus, the resulting updraft triggers deep convective clouds. The strong spatial correlation between the location of the first cloud cells and the convergence line indicates that the mass convergence is a key parameter in the triggering of the convection over the lee. This CI mechanism is similar to what has been reported by Barthlott et al. (2011) for the lee of the southern Black Forest peak, although, our case shows lower convective inhibition (CIN) in the primary-cell initiation point than they have reported (not shown). The heating of the near-surface air moreover increases the depth of the mixed layer and decreases the atmospheric stratification. Hence, no blocking effect is seen in Figure 6b; instead, the portion of the flow-over-the-mountain increases.

With increasing radiative forcing, the anabatic upslope, the background flow, and – in turn – the convergence lines intensify. Consequently, the convection deepens and precipitation forms (Figure 6c). The precipitation is accompanied by a cold outflow caused by evaporative cooling. The resulting cold pool is visible in the equivalent potential temperature (θ_e) contours. The cold and dry outflow lifts surrounding warm and moist air and generates secondary deep convection (Figure 6d). At first the primary cold pool propagates in all directions, but then it is stopped upstream by the mountain. Therefore, two groups of cloud clusters are observed two hours after precipitation onset which get separated by a downdraft core. The first one is attached to the mountain and the other one moves away from it (Figure 6e). The separation of the two updraft branches by a downdraft has also been observed for warm-season precipitation over the lee of northern Chinese mountains (Bao and Zhang, 2013). Thus, cold-pool dynamics play an important role in determining the precipitation pattern over the adjacent plain, besides the impact of mountain thermal circulations. Over the region swept by the cold pool, no further convection is triggered during the day (cf. Section 3.4). Shortly before 1500 LT, scattered convection caused by undisturbed PBL-growth is observed over FAR. This mechanism spreads a considerable amount of precipitation over the flat part of the domain (Figure 6e). In the evening (Figure 6e,f), when the surface energy fluxes diminish, convection decays likewise.

Although the typical flow features are similar for all days, significant day-to-day variability in the timing and location of the convection is seen. Figure 7 compares the diurnal equilibrium flow evolution with the evolution of an arbitrary day in terms of Liquid Water Path (LWP), accumulated precipitation, and near surface flow pattern. LWP is calculated as $\int_0^{p_s} \frac{q_c}{g}\, dp$, where p and p_s are the atmospheric and surface air pressure, q_c is the specific liquid water content and g is the acceleration of gravity.

The flow pattern on a specific day is much more irregular and less symmetric than the 20-day mean, in particular during the early morning and evening. This is due to the random outflow collisions all over the domain. The collision lines are visible through flow convergence and the consequent precipitation tracks. The spread between individual days is smaller during the period of strong thermal forcing in the morning and early afternoon.

We find that the flow evolution on individual days may deviate considerably from the mean flow. The flow is less symmetric around $y = 0$ mostly because cold pools propagate randomly throughout the domain. Nevertheless, the basic evolution such as lee-side triggering of deep convection, propagating cold pools, and convection suppression in the DRY region is repeated every day. In the next section we investigate the mechanisms responsible for the generation of the large differences between the three regions.

3.3 Initiation mechanisms for deep convection

Deep convection initiation requires three ingredients: first, a favorable environmental lapse rate, i.e. a conditionally unstable stratification; second, sufficient boundary-layer and mid-tropospheric moisture; and third, a triggering (e.g. lifting by convergence line, gravity current, PBL-growth, or topography) (Doswell et al., 1996). In other words, there should be sufficient convective available potential energy (CAPE) and some mechanisms to overcome CIN.

As mentioned in previous sections, the timing of the precipitation is different in different parts of the domain and so is the responsible mechanism for the convection triggering and deepening. The first convective activity after sunrise arises over the lee of the mountain (Figure 7d). Immediately before the first cell triggers, CIN decreases dramatically over the initiation point. This CI mechanism, which triggers along the convergence line generated by the up-slope flow confronting the background wind, is called "lee-convergence" (Banta, 1984; Banta, 1986). Subsequently, the cold-air outflow suppresses any further convective updrafts in this region. Instead, new cells trigger over the leading edge of the gust front (mountain-induced cold pool mechanism). Since the cold pool moving upstream cannot pass the mountain peak, it stays stationary, confronting the background

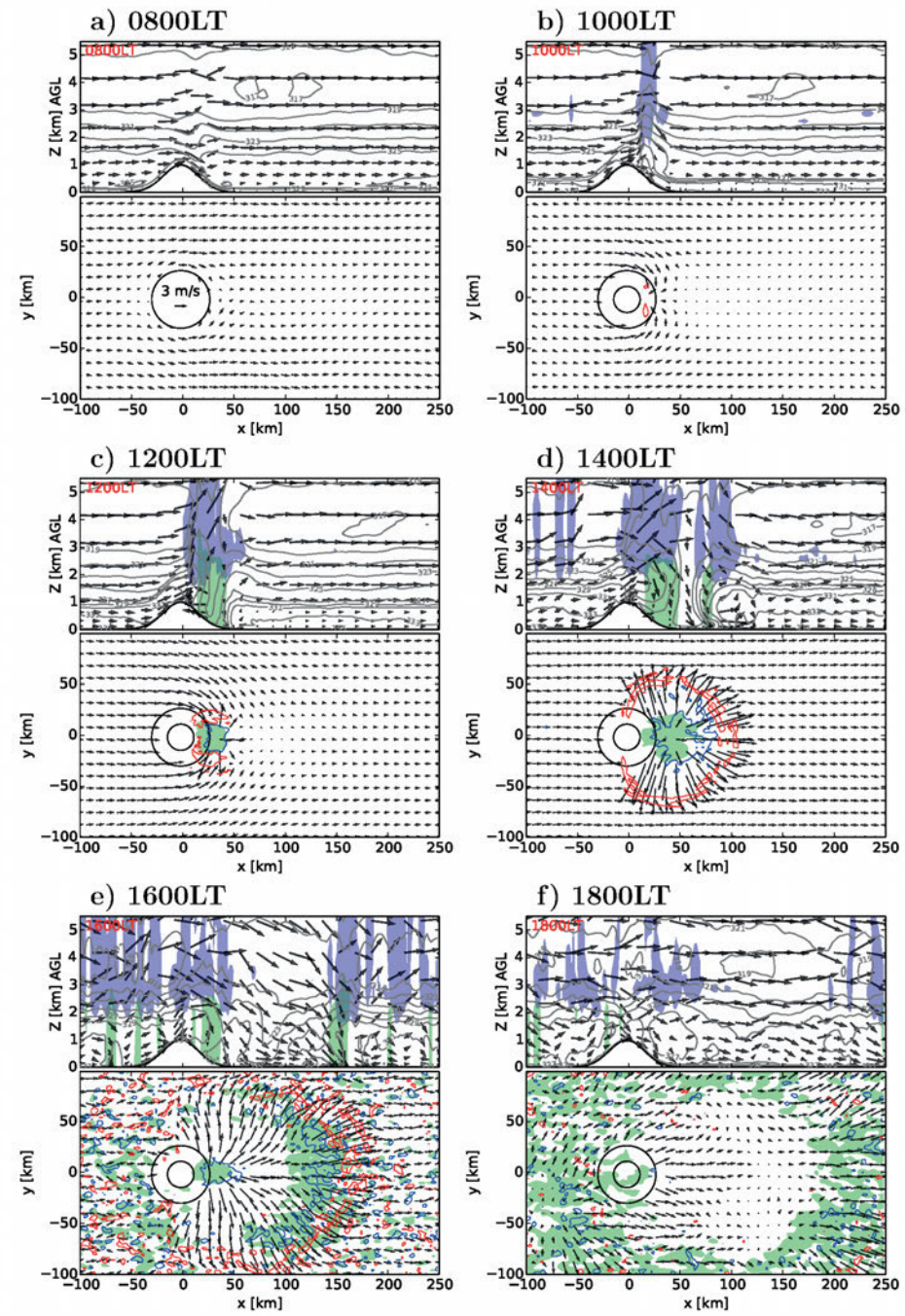

Figure 6: Summary of mean flow evolution in diurnal equilibrium (days 15–35) for the inner part of the domain; upper panels: vertical cross section of across mountain peak wind vectors, cloud liquid water (blue shading, threshold of 0.01 g kg^{-1}), precipitating water (green shading, threshold of 0.1 g kg^{-1}), equivalent potential temperature (gray lines, contour intervals of 2 K), and topography (black line). Lower panels: horizontal cross section of wind vectors at 250 m AGL, topography (black contours in 250 and 750 m AGL), accumulated surface precipitation of the last hour (green shading, threshold of 1 mm h^{-1}) and vertical wind at 750m AGL (upward motion in red and downward motion in blue contours with the amounts of 0.2 and -0.2 m s^{-1}).

flow. Therefore, clouds form two clusters; one which is attached to the mountain, and one arc-shaped propagating away from the mountain along with the front. This gust front leaves a cloud-free region behind (Figure 6e,f).

Apart from the locally triggered clouds over the near field, some random deep convection associated with surface-flux driven PBL-growth starts far enough from the mountain and is responsible for the late-afternoon precipitation over FAR (Figure 6e) starting around 1500 LT. Before the random deep convection triggers, CAPE reaches its highest value (1200–1500 J kg^{-1}) and CIN its lowest (3–15 J kg^{-1}) and the surface temperature approaches its convective temperature, T_c, over this region (more details in the next section). The randomly triggered convective cells over FAR in turn give

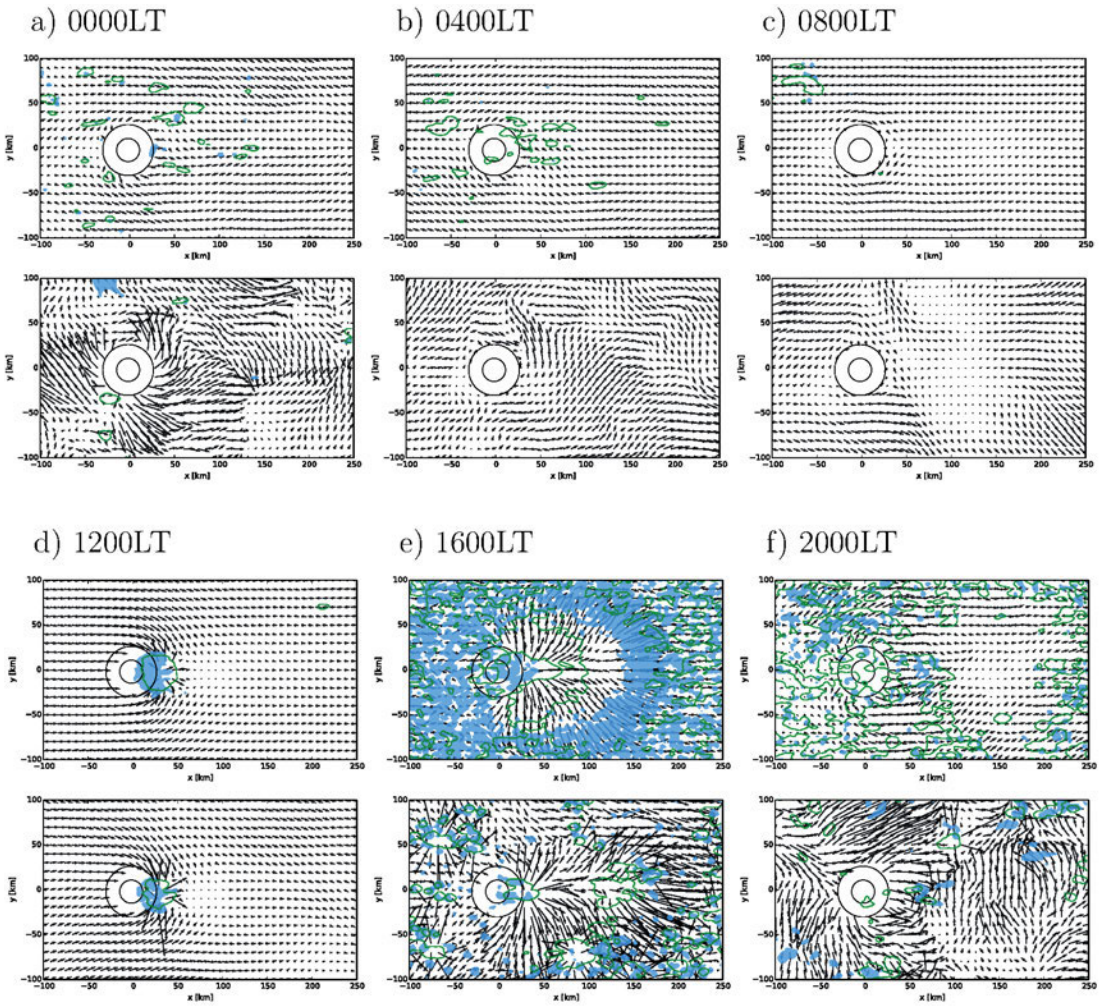

Figure 7: Comparison of mean flow evolution in the diurnal equilibrium phase (upper panels) against the specific flow at an arbitrary day (lower panels); panels show horizontal view of the Liquid Water Path (LWP; blue shading, threshold of 60 g m^{-2}) every 4 hours, wind vectors at 250 m AGL, accumulated surface precipitation over the last hour (green contours, threshold of 0.1 mm/h), and topography (black contours in 250 and 750 m AGL). In each frame, the upper panel is the 20-day mean and the lower panel is for one arbitrary day (day 19).

rise to precipitation and cold pools which trigger some new cells throughout the evening (1700–2100 LT) in a similar fashion as explained in Schlemmer and Hohenegger (2014). Since the location where the clouds develop and cold pools collide varies largely from one day to another, the updrafts are not clearly visible in the mean horizontal views, but for the individual days (Figure 7e,f). All the processes described above are repeated each day, with considerable day to day variability.

To summarize, lee-side convergence leads to an early onset of deep convection and precipitation (from 1000 LT) over WET, whereas the outflow-induced stabilization and drying of the PBL suppresses deep convection over DRY. Over FAR both undisturbed PBL-growth and evening cold-pool mechanisms are active. A key question still remains; why do the DRY regions remain cloud-free after the gust front passage? In other words, why is the undisturbed PBL-growth not initiated in this region after 1500 LT, similar as in FAR (see Figure 3–5)? In the next section we tackle this question by systematically analyzing the atmospheric profiles of DRY and FAR.

3.4 Generation of the DRY region

Figure 8a presents the DC of the mean values of potential temperature (θ) and specific humidity (q_v) within the lower boundary layer (lowest 50 hPa) over DRY and FAR. The differences in both quantities are substantial from 1200 LT to 1700 LT. From Figure 5 recall that the precipitation onset over FAR coincides with diminishing convective activities over DRY. The timing suggests that the deficit in θ and q_v over DRY is caused by the passage of the cold pool.

Figure 9 shows the hourly q_v budget over DRY for the time slice of interest. Before 1300 LT turbulence transports vapor from the surface and low levels upward closer to the top of the PBL. The presence of the cold-pool circulation is clearly visible at 1300 LT. At lower levels the horizontal advection of drier air leads to a drying of the lower PBL, while vertical advection of moist boundary-layer air associated with the updrafts over the leading edge of the cold pool leads to a moistening of a layer centered around 1.5–2 km. The cold-air advection also leads to a stable stratification of the lower PBL

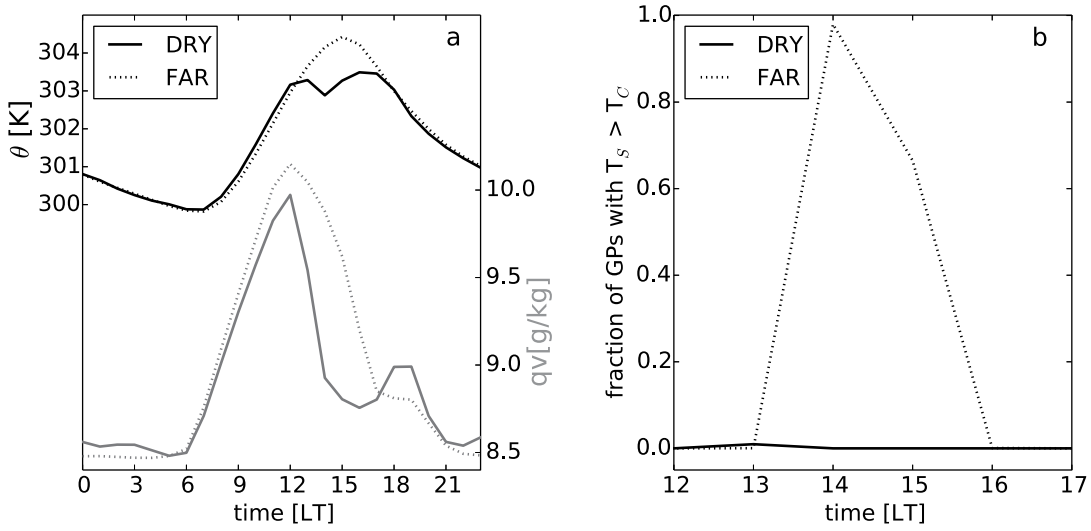

Figure 8: Mean diurnal cycle of (a) domain mean θ and q_v, within the lowest 50 hPa, and (b) the fraction of grid-points reaching their convective temperature T_c, in DRY and FAR.

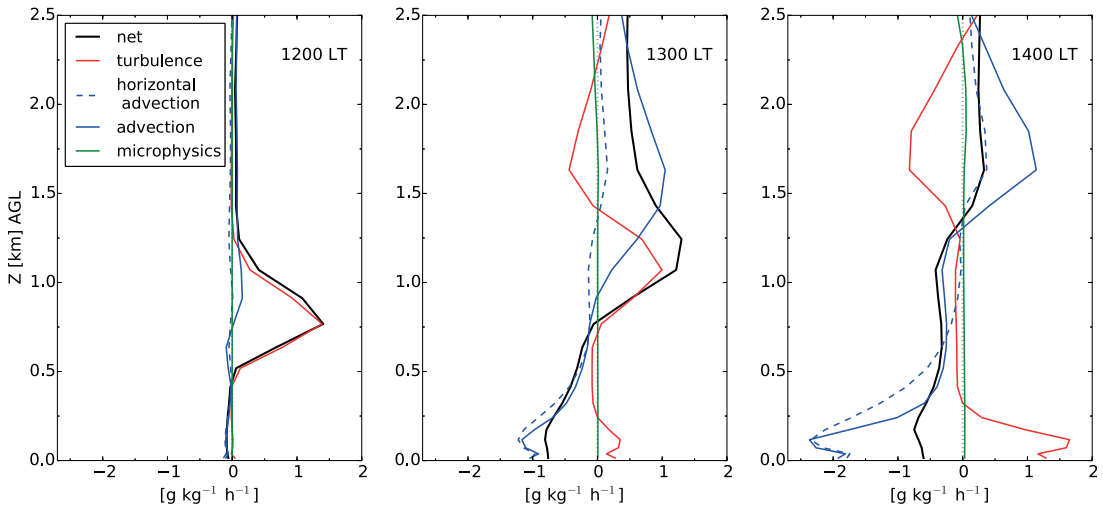

Figure 9: Domain mean q_v-tendency for the lowest 2.5 km AGL over DRY averaged over the 20 days in equilibrium.

(not shown). At 1400 LT surface-driven turbulence has started to remoisten the boundary layer. Yet the horizontal advection of dry air is still stronger leading to an overall negative tendency preventing a recovery of the PBL. Only after 1600 LT, the near-surface moisture content increases again (Figure 8a).

Figure 8b presents the fraction of the grid points in DRY and FAR that reach their convective temperature, T_c. The convective temperature in each grid-column is defined as the temperature an air parcel would have if it descended dry-adiabatically from the convective condensation level (CCL) to the surface. The CCL is defined as the lowest height at which the saturation mixing ratio equals the average mixing ratio of a 50-hPa deep near-surface layer. Apparently, the surface temperature is above T_c for 2–3 hours over FAR which causes the undisturbed PBL-growth mechanism to be active. However over DRY, hardly any grid point reaches its T_c over the same time period due to the presence of the cold pool. Consequently, when the rest of the flat part of the domain gets the late-afternoon precipitation, DRY remains almost cloud free and receives no precipitation.

3.5 Sensitivity to topographic height

3.5.1 Varying mountain heights

The previous analysis has shown that the topography significantly modifies the DC over different parts of the domain. So far, we have considered a mountain height of 1000 m. In this section, four additional experiments with different mountain heights (H = 125, 250, 500, and 2000 m) are conducted to investigate the influence of the mountain height on the timing and location of

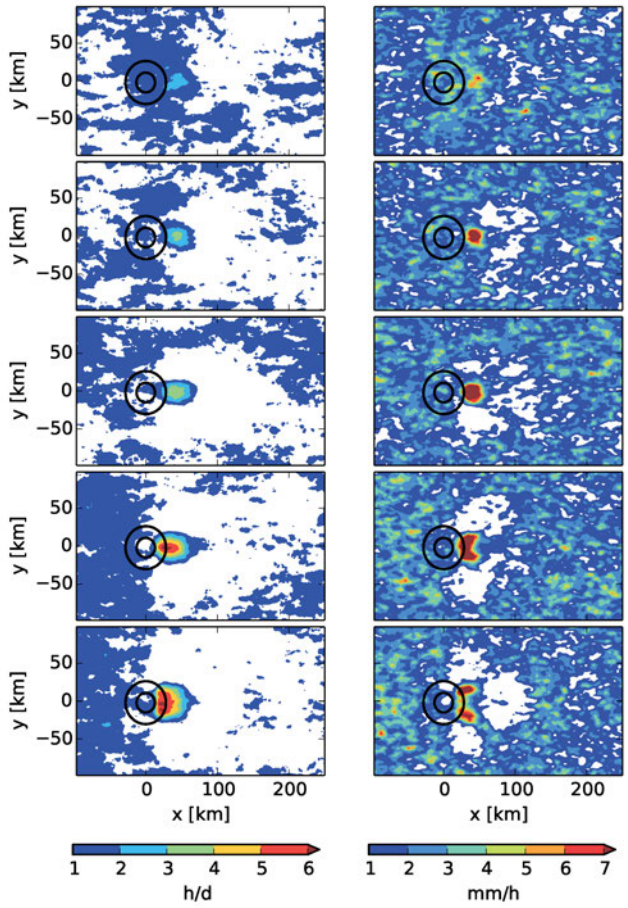

Figure 10: Mean surface precipitation frequency (left panel) and intensity (right panel) for experiments with different mountain heights (top to bottom, H = 125, 250, 500, 1000, and 2000 m). Frequency is defined as the number of wet hours (precipitation > 0.05 mm) per day, and intensity is the mean precipitation during wet hours.

the convective precipitation. The simulations are called H125, H250, H500, and H2000, respectively. Different heights can change the flow pattern and thereby affect the generation and evolution of deep convection.

In our setup, precipitation starts first over the mountain lee for all of the experiments, but the precipitation pattern, frequency, and intensity vary significantly. Figure 10 shows the mean frequency and intensity of the wet hours (defined as hours where the rain amounts exceeds 0.05 mm). The left panel presents the average number of wet hours per day over the last 20 days of the simulation and the right panel presents the corresponding precipitation intensity. The shape of the intensity cores changes from a single-peak core in H125 to a V-shaped core in H2000. This change of the shape of the precipitation pattern coincides with a change of the flow around the mountain in H125 to a flow over the mountain in H2000. In H1000 the portions of the air mass flowing over and around the mountain are comparable and the shape of the core remains arc-like. This is because of the number of the primary cells usually generated over the lee which is one for H125, H250, and H500 and is three and two for H1000 and H2000, respectively.

Figure 11 presents the dependency of the precipitation frequency and intensity maxima as well as the area of the most frequent and intense precipitation events of Figure 10 on the mountain height. For higher mountains, the frequency increases, indicating that the precipitation occurs over a longer time of the day. Also, the area having more than 5 wet hours per day is larger. The intensity on the other hand increases with height up to H500. From H1000 on, the splitting of the convective cores does not allow more precipitation accumulation over the lee. Hence, as soon as the primary convective cells split, the intensity maxima start to decrease. Nonetheless, the cores are so close to each other in H1000 that the area of the intense precipitation is still large. This area shrinks for H2000.

Figure 11b shows moreover that maximum precipitation intensity occurs for comparatively small mountains (500–1000 m) as seen in the area with high intensity shown in Figure 11d. This is consistent with the occurrence of vertical motion in the mountain airflow bifurcation (Schär and Durran, 1997) and also qualitatively consistent with observations of precipitation over the Hawaiian Islands (Smith et al., 2012).

3.5.2 Diurnal cycle of the flow regime and timing of precipitation onset

As discussed in the previous section the flow regime affects the amount and distribution of precipitation by regulating the portion of the flow directed over or around the mountain. The flow regime changes not only from case to case, but also over the course of the day for each case, through the diurnal forcing. Nevertheless, the determining atmospheric regime for the precipitation pattern is the regime established when the first convective cell triggers.

Generally, the atmosphere is in a stable state during the night. After sunrise, the boundary layer grows through sensible heating and the stability decreases. The more unstable the atmosphere gets, the larger the fraction of air that makes it over the mountain. Figure 12 shows the mean DC of the Brunt-Väisälä Frequency (N) and the non-dimensional mountain height ($\hat{h}$), which are the criteria used to define the flow regime. The values are integrated from the lowest atmospheric layer to the respective mountain height. This is done over FAR, where the flow is less disturbed by the mountain. For $\hat{h} \gg 1$, the atmospheric stratification is strong and the around-the-mountain flow dominates. For $\hat{h} \leq 1$, the stratification is weak or neutral and the over-the-mountain flow is dominant. With this definition, the atmosphere up to the mountain top is already unstable at 0800, 0900, 1000, and 1200 LT in H125, H250, H500, and H1000, respectively. But, it always stays stable for H2000. The stability increases again in the late afternoon in all of the cases redirecting the flow around the mountain.

Figure 13 presents the DC of the precipitation maximum, defined as the average over the 10 grid points

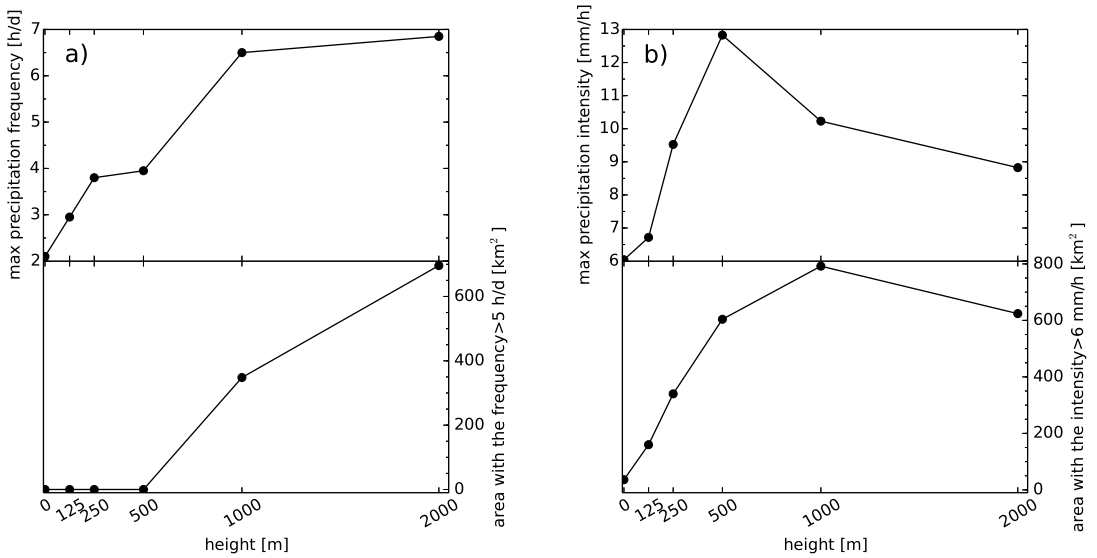

Figure 11: Variation of maximum precipitation frequency (top left) and maximum precipitation intensity (top right) with mountain height. Lower panels show the variation of the area with frequent ($> 5\,\mathrm{h\,d^{-1}}$) and intensive ($> 6\,\mathrm{mm/h^{-1}}$) precipitation with mountain height. The figure is based on the data shown in Figure 10.

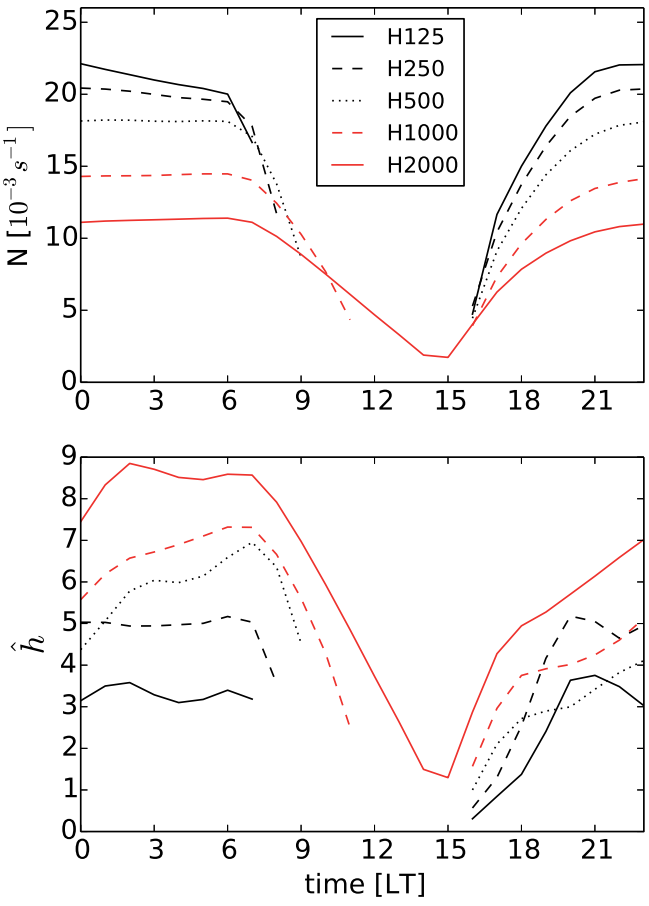

Figure 12: Mean diurnal cycle of domain mean static stability (N) and non-dimensional mountain height ($\hat{h} = N\,H/U$), where N and U are averaged between the lowest atmospheric layer and the mountain height over FAR. Values are suppressed for time periods with $N^2 < 0$.

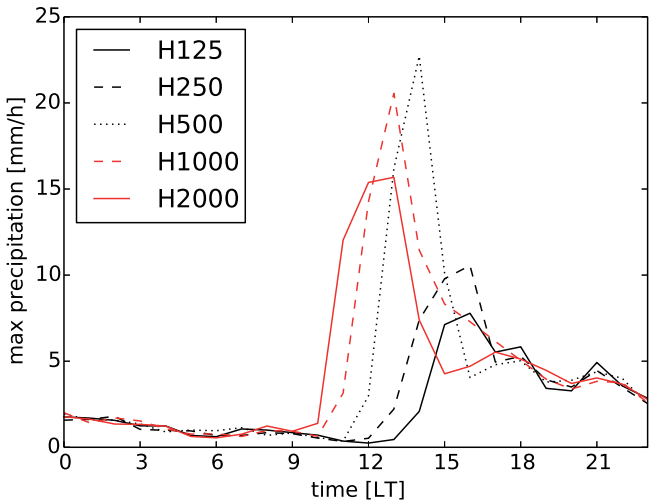

Figure 13: Diurnal cycle of the hourly mean surface maximum precipitation (averaged over the 10 grid points with the highest values).

with the highest precipitation amount in the domain. Apparently, the daytime maxima are associated with lee precipitation. The timing of the triggering of the first cells is affected by the topographic lifting and up-slope flow through the strengthened lee convergence. Both increase for higher topographies (Vergeiner and Dreiseitl, 1987). Thus, the precipitation onset is earlier over the higher mountains. The second reason for the earlier precipitation is that PBL development starts earlier over the higher topographies and the PBL height exceeds the LCL and LFC earlier, allowing for earlier deep convection. This is in line with the findings of Barthlott and Kirshbaum (2013). The value of the precipitation maxima is also a function of the flow regime. That is, they

increase with H in over-the-mountain regimes and decrease again for the cases with the primary-cell-split. This explains the results in Figure 11b. Apart from that, evening precipitation maxima diminish almost at the same rate for all the cases. Hence, earlier precipitation onset for higher topographies and almost the same termination time explain the increased precipitation frequency seen in Figure 11a.

4 Conclusions

The impact of an isolated mountain with a half-width of 20 km on summertime moist convection is investigated. The simulations are run for 35 days and after about 15 days a state of diurnal equilibrium is reached. This diurnal equilibrium state is characterized by repeating diurnal cycles and can be considered as an ensemble of single-day simulations with slightly different initial conditions.

Results show large spatial differences in the mean surface precipitation amount. While there is ample precipitation over the mountain lee slope (7.5 times the domain mean value), some adjacent regions only 40 km away get very little rain (0.25 times the domain mean value). Only far away from the mountain, the precipitation amounts approach the characteristics of the situation without topography.

It is shown that these spatial variations are generated by different convection initiation mechanisms over different parts of the domain. Over the lee, convection is triggered in the morning from the convergence of the anabatic mountain circulation and the background flow (lee-convergence). Convection triggered through this mechanism initiates a cold pool that propagates through the domain. In the direction facing the mountain, the cold pool remains stationary, while in the downstream direction, it propagates and numerous secondary convective cells are triggered along the leading edge. Some ten kilometers away from the lee-side precipitation maxima, no convection can be triggered because the cold pool dries and thus stabilizes the boundary layer. Over the flat part of the domain convective clouds form on top of a turbulent boundary layer. These cells deepen and organize into larger patterns due to cold-pool dynamics over the diurnal cycle.

The precipitation and convection show a very strong sensitivity with respect to the mountain height. The mountain height affects the precipitation onset by regulating the lee-convergence strength and the precipitation pattern by changing the flow regime. For higher mountains, the hourly precipitation frequency is increased due to the earlier triggering. However, the precipitation intensity is more dependent on the prevailing flow regime. Precipitation intensity increases with mountain height as long as the flow-over regime is dominant. Once the mountain height becomes sufficiently large to enforce a flow-around regime, precipitation intensity decreases due to the resulting splitting of the primary convective cell.

The current study aims at investigating the processes responsible for the summertime convection and precipitation over mid-latitude topography. Although the model and setup used are well suited for the current study, the role of additional factors such as interactive soil moisture, more complex environmental profiles, land-sea contrasts or more sophisticated mountain circulation effects are of interest. The current study will be continued spanning a larger parameter-space to better understand the role of the key factors that determine summertime convection over complex topography.

Acknowledgements

This research was supported by Swiss National Science Foundation (SNSF) grant 200021-132614. Special thanks are given to Steven Böing and the two anonymous reviewers for their insightful comments, which improved the quality of the paper. Authors are also grateful for technical support by Anne Roches and Daniel Lüthi. The numerical simulations have been performed on the Cray XC30 at the Swiss National Supercomputing Centre (CSCS) using the Consortium for Small-scale Modeling in climate mode (COSMO-CLM).

References

Addis, R.P., M. Garstang, G.D. Emmitt, 1984: Downdrafts from tropical oceanic cumuli. – Bound.-layer Meteor. **28**, 23–49, DOI: 10.1007/BF00119455.

Arakawa, A., W.H. Schubert, 1974: Interaction of a cumulus cloud ensemble with the large-scale environment, Part I.. – J. Atmos. Sci. **31**, 674–701, DOI: 10.1175/1520-0469(1974)031<0674:IOACCE>2.0.CO;2.

Baldauf, M., A. Seifert, J. Förstner, D. Majewski, M. Raschendorfer, T. Reinhardt, 2011: Operational convective-scale numerical weather prediction with the COSMO model: description and sensitivities. – Mon. Wea. Rev. **139**, 3887–3905, DOI: 10.1175/MWR-D-10-05013.1.

Banta, R.M., 1984: Daytime boundary-layer evolution over mountainous terrain. Part 1: Observations of the dry circulations. – Mon. Wea. Rev. **112**, 340–356, DOI: 10.1175/1520-0493(1984)112<0340:DBLEOM>2.0.CO;2.

Banta, R.M., 1986: Daytime boundary-layer evolution over mountainous terrain. Part 2: Numerical studies of upslope flow duration. – Mon. Wea. Rev. **114**, 1112–1130, DOI: 10.1175/1520-0493(1986)114<1112:DBLEOM>2.0.CO;2.

Banta, R.M., 1990: The role of mountain flows in making clouds. – In: Atmospheric processes over complex terrain, Meteor. Monogr. volume 23, 229–283.

Bao, X.H., F.Q. Zhang, 2013: Impacts of the mountain-plains solenoid and cold pool dynamics on the diurnal variation of warm-season precipitation over northern china. – Atmos. Chem. Phys. **13**, 6965–6982, DOI: 10.5194/acp-13-6965-2013.

Barthlott, C., N. Kalthoff, 2011: A numerical sensitivity study on the impact of soil moisture on convection-related parameters and convective precipitation over complex Terrain. – J. Atmos. Sci. **68**, 2971–2987, DOI: 10.1175/JAS-D-11-027.1.

Barthlott, C., D.J. Kirshbaum, 2013: Sensitivity of deep convection to terrain forcing over Mediterranean islands. – Quart. J. Roy. Meteor. Soc. **139**, 1762–1779, DOI: 10.1002/qj.2089.

Barthlott, C., R. Burton, D.J. Kirshbaum, K. Hanley, E. Richard, J. Chaboureau, J. Trentmann, B. Kern, H. Bauer, T. Schwitalla, C. Keil, Y. Seity, A. Gadian, A. Blyth, S. Mobbs, C. Flamant, J. Handwerker, 2011: Initiation of deep convection at marginal instability in an ensemble of mesoscale models: a case-study from COPS. – Quart. J. Roy. Meteor. Soc. **137**, 118–136, DOI: 10.1002/qj.707.

Bauer, M.H., G.J. Mayr, I. Vergeiner, H. Pichler, 2000: Strongly nonlinear flow over and around a three dimensional mountain as a function of the horizontal aspect ratio. – J. Atmos. Sci. **57**, 3971–3991, DOI: 10.1175/1520-0469(2001)058<3971:SNFOAA>2.0.CO;2.

Bennett, L.J., A.M. Blyth, R.R. Burton, A.M. Gadian, T.M. Weckwerth, A. Behrendt, P. Di Girolamo, M. Dorninger, S.J. Lock, V.H. Smith, S.D. Mobbs, 2011: Initiation of convection over the Black Forest mountains during COPS IOP15a. – Quart. J. Roy. Meteor. Soc. **137**, 176–189, DOI: 10.1002/qj.760.

Betts, A.K., 2000: Idealized model for equilibrium boundary layer over land. – J. Hydrometeor. **1**, 507–523, DOI: 10.1175/1525-7541(2000)001<0507:IMFEBL>2.0.CO;2.

Bott, A., 1989: A positive definite advection scheme obtained by nonlinear renormalization of the advective fluxes. – Mon. Wea. Rev. **117**, 1006–1016, DOI: 10.1175/1520-0493(1989)117<1006:APDASO>2.0.CO;2.

Crook, N.A., D.F. Tucker, 2005: Flow over heated terrain. Part I: Linear theory and idealized numerical simulations. – Mon. Wea. Rev. **133**, 2552–2564, DOI: 10.1175/MWR2964.1.

Demko, J.C., B. Geerts, 2010a: A numerical study of the evolving convective boundary layer and orographic circulation around the Santa Catalina mountains in Arizona. Part I: Circulation without deep convectin. – Mon. Wea. Rev. **138**, 1902–1922, DOI: 10.1175/2009MWR3098.1.

Demko, J.C., B. Geerts, 2010b: A numerical study of the evolving convective boundary layer and orographic circulation around the Santa Catalina mountains in Arizona. Part II: Interaction with deep convection. – Mon. Wea. Rev. **138**, 3603–3622, DOI: 10.1175/2010MWR3318.1.

Doms, G., J. Förstner, 2004: Development of a kilometer-scale NWP System: LMK. – COSMO Newsletter **4**, 159–167.

Doswell, C.A., H.E. Brooks, R.A. Maddox, 1996: Flash flood forecasting: An ingredients-based methodology. – Wea. Forecast. **11**, 560–581, DOI: 10.1175/1520-0434(1996)011<0560:FFFAIB>2.0.CO;2.

Durran, D.R., 1990: Mountain waves and downslope winds. – In: Atmospheric processes over complex terrain, Meteor. Monogr. volume 23, 59–81.

Eigenmann, R., N. Kalthoff, T. Foken, M. Dorninger, M. Kohler, D. Legain, G. Pigeon, B. Piguet, D. Schuttemeyer, O. Traulle, 2011: Surface energy balance and turbulence network during the Convective and Orographically-induced Precipitation Study (COPS). – Quart. J. Roy. Meteor. Soc. **137**, 57–69, DOI: 10.1002/qj.704.

Förstner, J., G. Doms, 2004: Runge-Kutta time integration and high-order spatial discretization of advection. A new dynamical core for the LMK. – COSMO Newsletter **4**, 168–176.

Fuhrer, O., C. Schär, 2005: Embedded cellular convection in moist flow past topography. – J. Atmos. Sci. **62**, 2810–2828, DOI: 10.1175/JAS3512.1.

Hagen, M., J. van Baelen, E. Richard, 2011: Influence of the wind profile on the initiation of convection in mountainous terrain. – Quart. J. Roy. Meteor. Soc. **137**, 224–235, DOI: 10.1002/qj.784.

Hauck, C., C. Barthlott, L. Krauss, N. Kalthoff, 2011: Soil moisture variability and its influence on convective precipitation over complex terrain. – Quart. J. Roy. Meteor. Soc. **137**, 42–56, DOI: 10.1002/qj.766.

Heise, E., M. Lange, B. Ritter, R. Schrodin, 2003: Improvement and validation of the multi-layer soil model. – COSMO Newsletter **3**, 198–203.

Hohenegger, C., P. Brockhaus, C. Schär, 2008: Towards climate simulations at cloud-resolving scales. – Meteorol. Z. **17**, 383–394, DOI: 10.1127/0941-2948/2008/0303.

Houze, R.A., 2012: Orographic effects on precipitating clouds. – Rev. Geophys. **50**, RG1001.

Kirshbaum, D.J., D.R. Durran, 2004: Factors governing cellular convection in orographic precipitation. – J. Atmos. Sci. **61**, 682–698, DOI: 10.1175/1520-0469(2004)061<0682:FGCCIO>2.0.CO;2.

Kirshbaum, D.J., R.B. Smith, 2008: Temperature and moist-stability effects on midlatitude orographic precipitation. – Quart. J. Roy. Meteor. Soc. **134**(33), 1183–1199, DOI: 10.1002/qj.274.

Kottmeier, C., N. Kalthoff, C. Barthlott, J. Corsmeier, U Van Baelen, A. Behrendt, R. Behrendt, A. Blyth, R. Coulter, P. Crewell, S. Di Girolamo, M. Dorninger, C. Flamant, T. Foken, M. Hagen, H. Hauck, C Holler, H. Konow, M. Kunz, H. Mahlke, S. Mobbs, R. Richard, E. Steinacker, T. Weckwerth, A. Wieser, V. Wulfmeyer, 2008: Mechanisms initiating deep convection over complex terrain during COPS. – Meteorol. Z. **17**, 931–948, DOI: 10.1127/0941-2948/2008/0348.

Mayr, G.J., L. Armi, 2010: The influence of downstream diurnal heating on the descent of flow across the Sierras. – J. Appl. Meteor. Climatol. **49**, 1906–1912, DOI: 10.1175/2010JAMC2516.1.

Miglietta, M.M., A. Buzzi, 2001: A numerical study of moist stratified flows over isolated topography. – Tellus Ser. A-Dyn. Met. Oce. **53**, 481–499, DOI: 10.1111/j.1600-0870.2001.00481.x.

Miglietta, M.M., A. Buzzi, 2004: A numerical study of moist stratified flow regimes over isolated topography. – Quart. J. Roy. Meteor. Soc. **130**, 1749–1770, DOI: 10.1256/qj.02.225.

Miglietta, M.M., R. Rotunno, 2009: Numerical simulations of conditionally unstable flows over a mountain ridge. – J. Atmos. Sci. **66**, 1865–1885, DOI: 10.1175/2009JAS2902.1.

Mironov, D., M. Raschendorfer, 2001: Evaluation of empirical parameters of the new LM surface-layer parameterization scheme. – COSMO technical report.

Parker, D.J., 1996: Cold pools in shear. – Quart. J. Roy. Meteor. Soc. **112**, 1655–1674, DOI: 10.1256/smsqj.53508.

Peixoto, J.P., A.H. Oort, 1996: The climatology of relative humidity in the atmosphere. – J. Climate **9**, 3443–3463, DOI: 10.1175/1520-0442(1996)009<3443:TCORHI>2.0.CO;2.

Queney, P., 1948: The problem of air flow over mountains: A summary of theoretical results. – Bull. Amer. Meteor. Soc. **29**, 16–26.

Raschendorfer, M., 2001: The new turbulence parameterization of LM. – COSMO Newsletter **1**, 90–98.

Reinhardt, T., A. Seifert, 2006: A three-category ice scheme for LMK. – COSMO Newsletter **6**, 115–120.

Ritter, B., J.F. Geleyn, 1992: A comprehensive radiation scheme for numerical weather prediction models with potential applications in climate simulations. – Mon. Wea. Rev. **120**, 303–325, DOI: 10.1175/1520-0493(1992)120<0303:ACRSFN>2.0.CO;2.

Roe, G.H., 2005: Orographic precipitation. – Annual Review of Earth and Planetary Sciences **33**, 645–671, DOI: 10.1146/annurev.earth.33.092203.122541.

Rotunno, R., J.B. Klemp, M.L. Weisman, 1988: A theory for strong, long-lived squall lines. – J. Atmos. Sci. **45**, 463–485, DOI: 10.1175/1520-0469(1988)045<0463:ATFSLL>2.0.CO;2.

Schär, C., 2001: Mesoscale mountains and the synoptic-scale atmospheric dynamics: A review. – In: Meteorology at the Millennium: 150th Anniversary Conference of the Royal Meteorological Society, volume 23, Academic Press, 29–42.

Schär, C., D.R. Durran, 1997: Vortex formation and vortex shedding in continuously stratified flows past isolated topography. – J. Atmos. Sci. **54**, 534–554, DOI: 10.1175/1520-0469(1997)054<0534:VFAVSI>2.0.CO;2.

Schlemmer, L., C. Hohenegger, 2014: The formation of wider and deeper clouds as a result of cold-pool dynamics. – J. Atmos. Sci. **71**, 2842–2858, DOI: 10.1175/JAS-D-13-0170.1.

Schlemmer, L., C. Hohenegger, J. Schmidli, C.S. Bretherton, C. Schär, 2011: An idealized cloud-resolving framework for the study of midlatitude diurnal convection over land. – J. Atmos. Sci. **68**, 1041–1057, DOI: 10.1175/2010JAS3640.1.

Schlemmer, L., C. Hohenegger, J. Schmidli, C. Schär, 2012: Diurnal equilibrium convection and land surface-atmosphere interactions in an idealized cloud-resolving model. – Quart. J. Roy. Meteor. Soc. **138**, 1526–1539, DOI: 10.1002/qj.1892.

Schneidereit, M., C. Schär, 2000: Idealised numerical experiments of Alpine flow regimes and southside precipitation events. – Meteor. Atmos. Phys. **72**, 233–250, DOI: 10.1007/s007030050018.

Smith, R.B., 1979: The Influence of mountains on the atmosphere. – Adv. Geophys. **21**, 87–230.

Smith, R.B., I. Barstad, 2004: A linear theory of orographic precipitation. – J. Atmos. Sci. **61**, 1377–1391, DOI: 10.1175/1520-0469(2004)061<1377:ALTOOP>2.0.CO;2.

Smith, R.B., S. Gronas, 1993: Stagnation points and bifurcation in 3-D mountain airflow. – Tellus Ser. A-Dyn. Met. Oce. **45**, 28–43, DOI: 10.1034/j.1600-0870.1993.00003.x.

Smith, R.B., J.R. Minder, A.D. Nugent, T. Storelvmo, D.J. Kirshbaum, R. Warren, N. Lareau, P. Palany, A. James, J. French, 2012: Orographic precipitation in the tropics: The Dominica Experiment. – Bull. Amer. Meteor. Soc. **93**, 1567–1579, DOI: 10.1175/BAMS-D-11-00194.1.

Steppeler, J., G. Doms, U. Schättler, H.W. Bitzer, A. Gassmann, U. Damrath, G. Gregoric, 2003: Meso-gamma scale forecasts using the nonhydrostatic model LM. – Meteor. Atmos. Phys. **82**, 75–96, DOI: 10.1007/s00703-001-0592-9.

Tompkins, A.M., 2001: Organization of tropical convection in low vertical wind shears: The role of cold pools. – J. Atmos. Sci. **58**(59), 1650–1672, DOI: 10.1175/1520-0469(2001)058<1650:OOTCIL>2.0.CO;2.

Van Baelen, J., M. Reverdy, F. Tridon, L. Labbouz, G. Dick, M. Bender, M. Hagen, 2011: On the relationship between water vapour field evolution and the life cycle of precipitation systems. – Quart. J. Roy. Meteor. Soc. **137**, 204–223, DOI: 10.1002/qj.785.

Vergeiner, I., E. Dreiseitl, 1987: Valley winds and slope winds - observations and elementary thoughts. – Meteorol. Atmos. Phys. **36**, 264–286, DOI: 10.1007/BF01045154.

Weaver, J.F., S.P. Nelson, 1982: Multiscale aspects of thunderstorm gust fronts and their effects on subsequent storm development. – Mon. Wea. Rev. **110**, 707–718, DOI: 10.1175/1520-0493(1982)110<0707:MAOTGF>2.0.CO;2.

Wicker, L.J., W.C. Skamarock, 2002: Time splitting methods for elastic models using forward time schemes. – Mon. Wea. Rev. **130**, 2088–2097, DOI: 10.1175/1520-0493(2002)130<2088:TSMFEM>2.0.CO;2.

Wulfmeyer, V., C. Flamant, A. Behrendt, A. Blyth, A. Brown, M. Dorninger, A. Illingworth, P. Mascart, A. Montani, T. Weckwerth, 2011: Advances in the understanding of convective processes and precipitation over low-mountain regions through the Convective and Orographically-induced Precipitation Study (COPS). – Quart. J. Roy. Meteor. Soc. **137**, 1–2, DOI: 10.1002/qj.799.

Young, G.S., S.M. Perugini, C.W. Fairall, 1995: Convective wakes in the equatorial western Pacific during TOGA. – Mon. Wea. Rev. **123**, 110–123, DOI: 10.1175/1520-0493(1995)123<0110:CWITEW>2.0.CO;2.